Engineering Structures 56 (2013) 1557–1569

Contents lists available at ScienceDirect

Engineering Structures

journal homepage: www.elsevier.com/locate/engstruct

Seismic behavior of steel reinforced concrete column–steel truss beam hybrid joints

Mu-Xuan Tao *, Jian-Sheng Fan, Jian-Guo Nie

Key Laboratory of Civil Engineering Safety and Durability of China Education Ministry, Dept. of Civil Engineering, Tsinghua University, Beijing 100084, China

ARTICLE INFO

Article history:
Received 14 October 2012
Revised 19 July 2013
Accepted 22 July 2013

Keywords:
Hybrid joint
Steel reinforced concrete column
Steel truss beam
Seismic behavior
Experimental study
Failure mode
Shear strength
Joint core

ABSTRACT

A research program on seismic behavior of steel reinforced concrete column–steel truss beam hybrid joints is carried out to support the design of the New China Science & Technology Museum built at Beijing City. Reversed cyclic loading tests on four specimens are first conducted to intensively investigate the seismic behavior of the hybrid joint. The load–displacement curves, shear behavior of the joint core, strength and stiffness degradations, ductility, energy dissipation capacity, deformation characteristics, etc. of the test subassemblies are analyzed. Two different failure modes can be observed in the tests, and the joints with flexural failure at the beam end illustrate higher stiffness and strength, better ductility and energy dissipation capacity than those with shear failure at the joint core. As a result, rational control of the failure mode is one of the most effective ways to enhance the seismic behavior of the joint. Based on the experimental observations, a design formula for shear strength of the joint core is derived using the shear model including the inner concrete compression strut, outer concrete compression strut and steel web panel shear mechanisms, and an analytical method for controlling the failure mode of the joint is also presented. Finally, the proposed method in this paper is verified by the experiment results and compared with other available methods provided in the current design codes and the literature.

1. Introduction

The New China Science & Technology Museum is one of the most important auxiliary projects for the 2008 Olympic Game in Beijing. In order to satisfy the high-standard requirements of exhibition function and seismic fortification, a hybrid structural system composed of a large-span spatial steel truss structure and a steel reinforced concrete frame-shear wall structure as shown in Fig. 1 is adopted. Since the two types of structures have entirely different mechanical properties, the seismic behavior of the hybrid joint connecting these two different structures as illustrated in Fig. 1a dominates the seismic performance of the whole structural system and becomes one of the most critical problems for design.

The steel–concrete hybrid joints in the hybrid structural system investigated in previous researches [1–5] mainly include the reinforced concrete column–steel beam (RC–S) hybrid joint and the steel reinforced concrete column–steel beam (SRC–S) hybrid joint.

RC–S hybrid joints were firstly tested by Sheikh et al. [6] and Deierlein et al. [7] in 1989 at University of Texas, and then tested by Kanno and Deierlein [8] in 1993 at Cornell University. All the obtained test data formed the basis of the first design guidelines provided by the ASCE Task Committee on Design Criteria for Composite Structures in Steel and Concrete [9] in the United States in 1994. After that, the US–Japan Cooperative Research Program on Composite and Hybrid Structures was carried out [10], and one of the most important aims of this program was to develop improved seismic design models and criteria for RC–S beam–column connection subassemblies. In the US, a series of tests were conducted by many researches (e.g., Parra-Montesinos and Wight [11]; Parra-Montesinos et al. [12]; Fargier-Gabaldón and Parra-Montesinos [13]), and improved models for shear behavior of the joint core were also proposed [12,14]. In addition, these models have been applied to the design and modeling of a beam–column sub-structure [15] and a whole hybrid structural system [16]. In Japan, guidelines for the seismic design of hybrid RC–S joints [17] were formed through the investigations of the joint stress transferring mechanism [18] and the elaborate finite element simulation [19], etc.

In addition to the RC–S hybrid joint, the SRC–S hybrid joint is also popular in innovative hybrid structural systems at seismic zones. Experimental and analytical studies were carried out by Chou and Uang [20], Weng et al. [21], and Seo et al. [22] and design guidelines for the hybrid SRC–S joint were provided by the Architectural Institute of Japan (AIJ) [23].

In spite of the extensive studies of hybrid joints in the literature, the topics on the seismic performance and design method of the steel reinforced concrete column–steel truss beam hybrid joint still have not been fully addressed since all the steel beams concerned in previous researches are only in the solid web type. In addition,

* Corresponding author. Tel.: +86 10 13810486510.
E-mail address: taomuxuan@tsinghua.edu.cn (M.-X. Tao).

0141-0296/$ - see front matter © 2013 Published by Elsevier Ltd.
http://dx.doi.org/10.1016/j.engstruct.2013.07.029

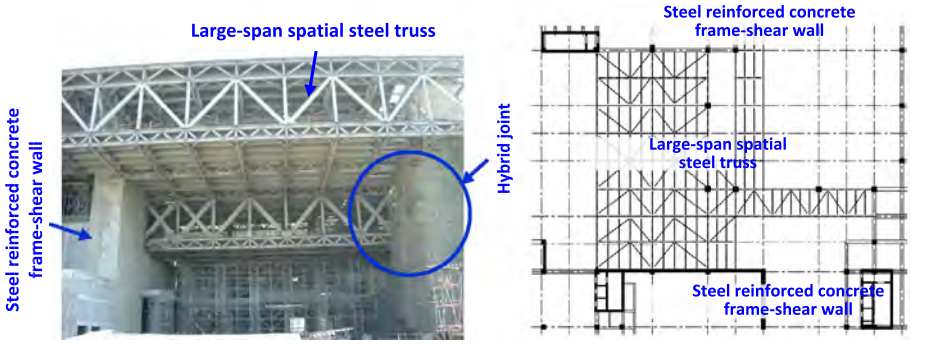

(a) Construction site (b) Typical floor plan (Second floor at West Gate)

Fig. 1. The New China Science & Technology Museum.

since the stiffness and loading capacity of the steel truss beam are relatively large due to the large section height for realizing the long span compared to the steel solid web beam usually used in the routine frame floor, it may be not easy to achieve the strong joint core/weak member design goal. As a result, the shear design of the joint core and the rational control of the failure mode may dominate the whole design procedure of the joint. However, the design formula for the shear strength of this type of hybrid joint core and the effective approach for controlling the failure mode to improve the seismic ductility of the joint for design purpose are not available in the literature and current design codes.

In this paper, reversed cyclic loading tests of four steel reinforced concrete column–steel truss beam hybrid joint specimens divided into two groups are first carried out to investigate seismic performance of the joint. The load–displacement curves, shear behavior of the joint core, strength and stiffness degradations, ductility, energy dissipation capacity, deformation characteristics and beam-end flexural behavior of the test subassemblies are discussed in detail, and the influence of different failure modes on the seismic behavior of the joints is concentrated on. Furthermore, the equilibrium equations of the ultimate external forces and internal effective shear strengths are derived. A design formula for shear strength of the joint core is proposed using the shear model including the inner compression concrete strut, outer compression concrete strut and steel web panel shear mechanisms [14], and an analytical method for controlling the failure mode of the joint is also presented. Finally, the proposed method in this paper is verified by the experiment results and compared with other methods provided in the current design codes and the literature. In addition, the contributions of the three mechanisms to the shear strength of the joint core are also evaluated by the proposed design formula in this paper.

2. Experimental program

2.1. Specimen design

Two typical hybrid joints located at the 2nd floor of the west gate of New China Science & Technology Museum (designated as SRCTJ1 and SRCTJ2, respectively) are selected for the scale model tests. The detailed dimensions of the specimens are illustrated in Fig. 2. The steel truss beam depths of all the specimens are the same, but the depth of the SRCTJ1's column section is twice larger than that of the SRCTJ2's so that different failure modes may be expected in tests. The SRCTJ1 and SRCTJ2 each have two specimens with different shear stud arrangements but the same dimensions. Shear studs are arranged along the whole SRC columns for the specimens SRCTJ1-1 and SRCTJ2-1 whereas only in the joint core regions for the specimens SRCTJ1-2 and SRCTJ2-2 as shown in Figs. 2 and 3a. Assuming that the positions of the inflection points are determined from the results of the global structural analysis, a tee-shaped subassembly along with boundary and loading conditions can simulate part of a structure subjected to an earthquake-induced moment. In considerations of the available maximum loading capacity of the actuator and the conditions of the laboratory, the scale ratio of the specimens is finally determined as 1:3.

2.2. Fabrication and material properties

Fig. 3 shows the fabrication procedure of the specimens including the fabrication of steel structures, assembling of reinforcement and pouring of concrete. The mechanical properties of the steel and reinforcement materials obtained from the material property tests are given in Table 1. The average cubic compressive strengths of the column concrete (the side length of the standard cubic specimens = 150 mm) obtained on the same day the joints are tested are 42.8 MPa for SRCTJ1-1 and SRCTJ1-2, 44.1 MPa for SRCTJ2-1, and 46.8 MPa for SRCTJ2-2.

2.3. Test setup and loading procedure

As shown in Fig. 4, the steel reinforced concrete column is in the horizontal direction and the steel truss beam is in the vertical direction. The one end of an actuator is connected to the top end of the beam, and the other end is connected to the reaction wall. Four triangular supports are used as lateral support devices to constrain the out-of-plane deformation of the specimens. The column is anchored to the laboratory base at the inflection points, and its longitudinal displacement is also constrained. In the test, horizontal force is imposed using the force-control scheme repeated only once at each control point before the specimen yields and then using the displacement-control scheme repeated twice at each control point after the specimen yields.

2.4. Measuring devices

Fig. 5a gives the arrangement of main measuring devices in detail. The displacement meter D2 is arranged to obtain the horizontal displacement at the truss beam end, which reflects the summation of beam deformation, column deformation and total joint deformation. The displacement meter D3 is used to modify the beam end displacement considering the influence of horizontal slip at the column anchorage points. In order to investigate the shear performance of the joint core, twin extensometers E4 and E5 are arranged diagonally to measure the shear deformation of the core region. Since the semi-rigidity of this kind of joint can be neglected, the joint shear deformation derived from the twin

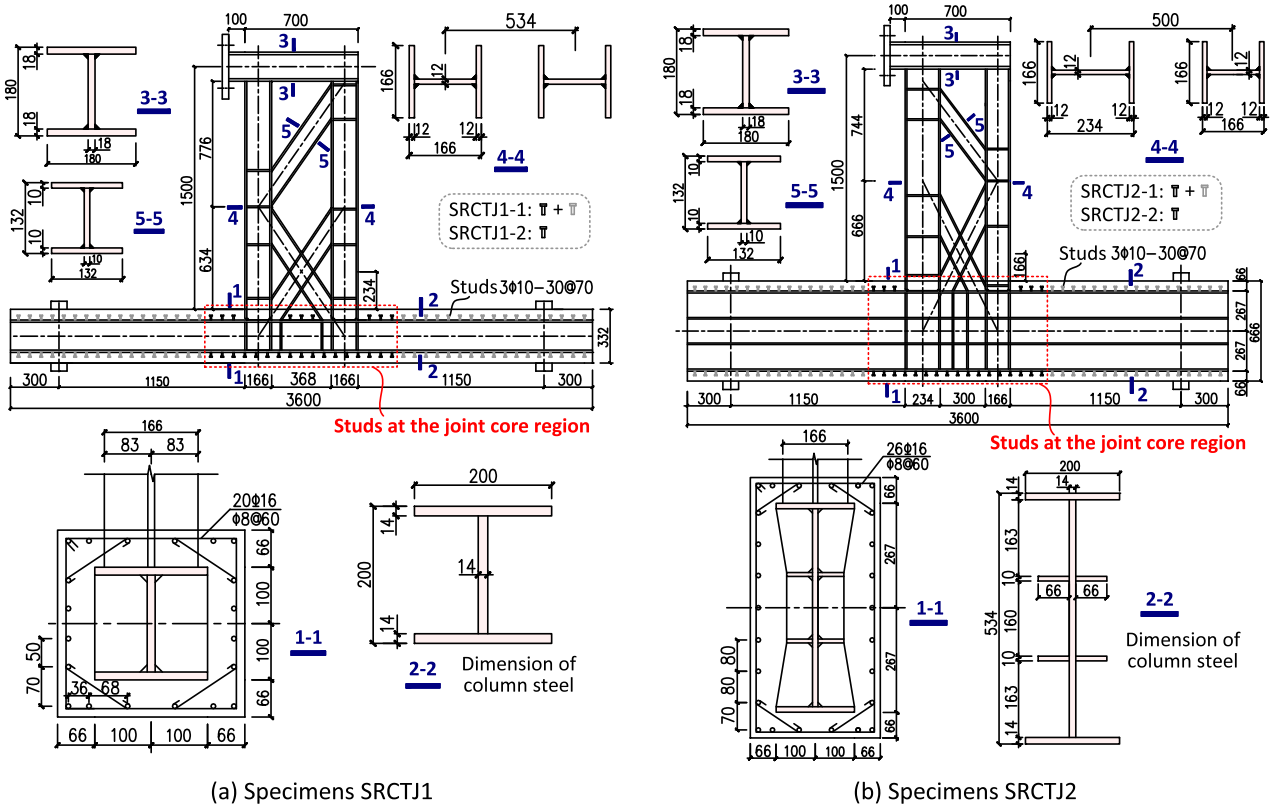

Fig. 2. Detailed parameters of specimens.

Fig. 3. Fabrication of specimens.

Table 1
Mechanical properties of the steel and reinforcement materials (average values).

	Usage	Yield strength (MPa)	Ultimate strength (MPa)	Elongation (%)	Ultimate strength/yield strength
10 mm-thick steel plate	Diagonal web members of steel truss beam	341.3	505.3	31.1	1.48
12 mm-thick steel plate	Upper and lower chords of steel truss beam	339.6	518.9	45.0	1.53
14 mm-thick steel plate	Embedded steel column	348.6	539.0	27.3	1.55
ϕ8 reinforcement	Column hoop reinforcement	323.1	432.4	–	1.34
ϕ16 reinforcement	Column longitudinal reinforcement	372.3	543.3	–	1.46

Fig. 4. Test setup.

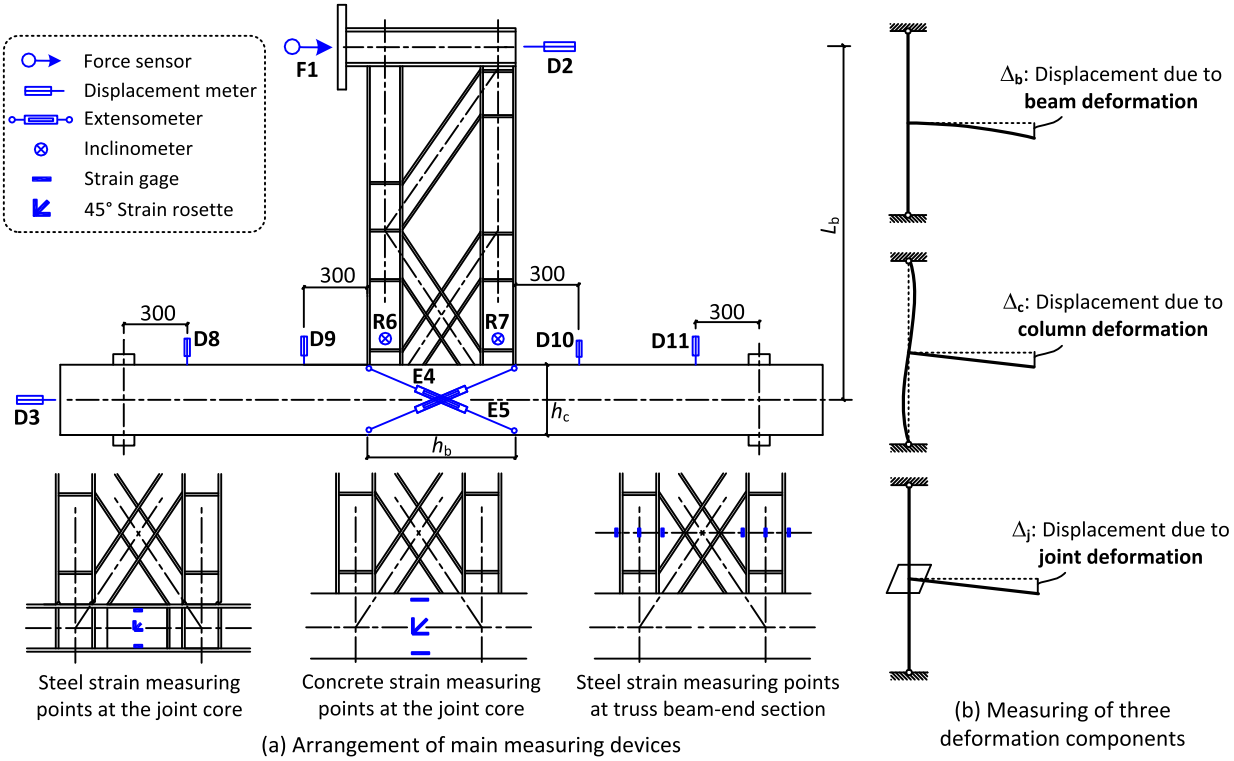

Fig. 5. Measuring scheme of the test.

extensometers can approximately represent the total joint deformation. Inclinometers R6 and R7 are used to monitor the beam rotation adjacent to the joint core so that the summation of the column deformation and the joint deformation can be calculated indirectly. Four displacement meters D8–D11 are also arranged to measure the column deformation.

When a subassembly is loaded, the displacement at the beam end is composed of the displacement due to the beam deformation

Δ_b, the displacement due to the column deformation Δ_c, and the displacement due to the joint deformation Δ_j as illustrated in Fig. 5b. These three displacement components can be determined from the measuring results of D2, D3, E4, E5, R6 and R7 using the following equations:

$$\Delta_j = \frac{0.5(E_4 + E_5)\sqrt{h_b^2 + h_c^2}}{h_b \cdot h_c} L_b \quad (1)$$

$$\Delta_c = \left[0.5(R_6 + R_7) - \frac{0.5(E_4 + E_5)\sqrt{h_b^2 + h_c^2}}{h_b \cdot h_c}\right] L_b \quad (2)$$

$$\Delta_b = D_2 - D_3 - 0.5(R_6 + R_7)L_b \quad (3)$$

where h_b is the depth of steel truss beam; h_c is the depth of SRC column; and L_b is the beam length as shown in Fig. 5a.

In addition, steel and concrete strain rosettes are arranged at the joint core to intensively investigate the development of shear deformation at the joint core, and some longitudinal steel strain gages are also arranged at a critical beam-end section to monitor the beam-end flexural behavior as illustrated in Fig. 5a. The distribution and development of the concrete cracks are also monitored in the test.

3. Experimental results

3.1. General behavior

3.1.1. SRCTJ1 series

Since both specimens of the SRCTJ1 series demonstrate similar phenomenon in the tests, only the specimen SRCTJ1-2 is discussed here.

In the force-control loading stage, when the lateral force reaches positive 600 kN, large amounts of diagonal cracks appear at the joint core. Then the opposite loading to negative 600 kN results in densely distributed crossed diagonal cracks at the joint core and the yielding of the specimen indicated by the load–displacement curve. The cracking pattern at this time as shown in Fig. 6a can give valuable evidence for selecting a reasonable inclined angle of the concrete compression strut in the shear modeling of the joint core. In the displacement-control loading stage after the specimen yields, when the applied displacement firstly reaches positive 55 mm (corresponding to the drift angle of 33.3 mrad), the concrete at the joint core begins to crush. After that, the area of the crushing concrete is gradually expanding with the increasing of the displacement amplitude. Finally, the shear failure of the joint core illustrated as Fig. 6b can be observed when the positive applied displacement reaches about 100 mm (corresponding to the drift angle of 58.8 mrad).

3.1.2. SRCTJ2 series

Since both specimens of the SRCTJ2 series demonstrate similar phenomenon in the tests, only the specimen SRCTJ2-2 is discussed here.

In the force-control loading stage, similar diagonal cracking pattern as SRCTJ1 series is formed at the joint core as illustrated in Fig. 6c. However, in the displacement-control loading stage after the specimen yields, no evident crack development at the joint core can be observed. When the applied displacement reaches positive 80 mm (corresponding to the drift angle of 43.5 mrad), local buckling of the steel compressive flange adjacent to the joint core region occurs. Finally, a typical flexural failure with a plastic hinge formed at the truss beam end near the beam–column surface, where the compressive steel flange locally buckles and the diagonal web member fractures near the weld heat-affect zone, can be observed as shown in Fig. 6d.

3.2. Load–displacement curve

The load–displacement hysteretic and skeleton curves of the specimens are shown in Fig. 7. The hysteretic loops of all the specimens are plump, and the curves of the SRCTJ2 series demonstrate higher loading capacity, stiffness and energy dissipation capacity than those of the SRCTJ1 series, indicating that the seismic behavior of the strong joint core-weak beam subassemblies with flexural

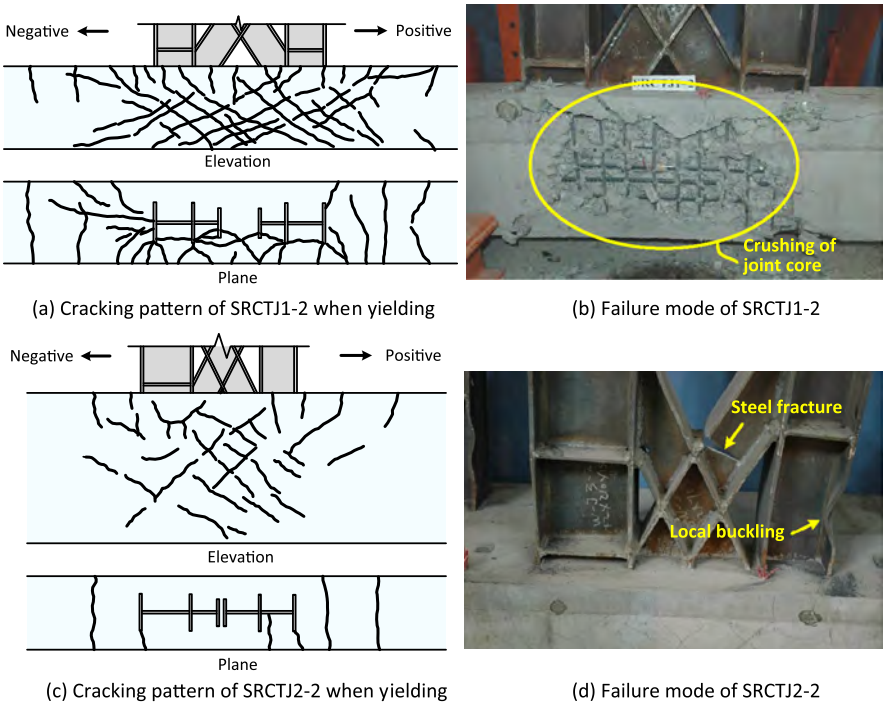

(a) Cracking pattern of SRCTJ1-2 when yielding

(b) Failure mode of SRCTJ1-2

(c) Cracking pattern of SRCTJ2-2 when yielding

(d) Failure mode of SRCTJ2-2

Fig. 6. General behavior of specimens.

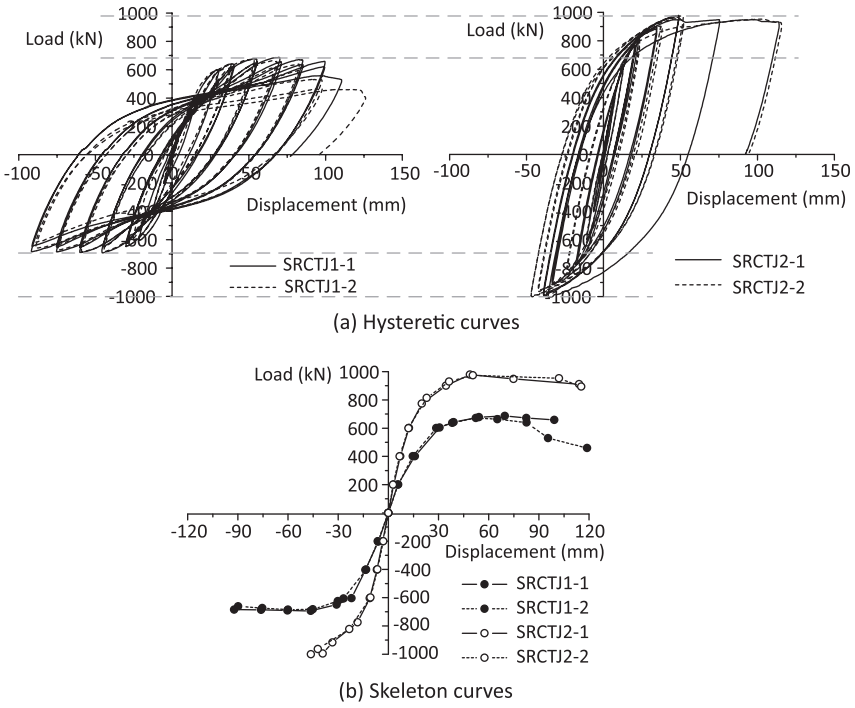

Fig. 7. Load–displacement curves.

failure at the truss beam end is superior to that of the weak joint core-strong beam ones. In addition, the coincidence of the curves of the twin SRCTJ1 (or SRCTJ2) specimens indicates that the composite action can be achieved through the natural cohesion between the steel and concrete for the steel reinforced concrete column in the hybrid subassembly no matter whether the shear studs are arranged or not.

Three critical characteristic points, namely, yield point, ultimate point and failure point can be obtained from the skeleton curves as shown in Fig. 8, and the characteristic loads and displacements corresponding to these three points are listed in Table 2. The yield point (P_y, Δ_y) can be determined using the graphical method in Ref. [24] as shown in Fig. 8. The ultimate load P_u is selected as the maximum load, and the failure displacement Δ_f is defined as the maximum displacement corresponding to the load no less than $0.85P_u$.

3.3. Shear behavior of joint core

The global shear behavior of the joint core is illustrated as Fig. 9a, where Q_j and γ_j represent the shear force and the average shear deformation of the joint core, respectively. The curves of the SRCTJ1 are stable and energy dissipative, indicating the shear failure of the joint core. The curves of the SRCTJ2 demonstrate that the shear deformation developed insufficiently since the failure mode of these joints is the flexural failure at the beam end.

In addition, the center point at the steel web panel is also equipped with a 3-axis rosette to measure the shear strain. Fig. 9b shows the comparison between the global and local shear behavior of the joint core for the specimens SRCTJ1-1 and SRCTJ1-2. A good correlation between the shear force-average shear deformation hysteretic curve and the shear force-center point shear strain hysteretic curve indicates that the shear deformation at the center point of the steel web panel can represent the average shear deformation of the whole joint core. As a result, when the shear strength of the joint core is evaluated, full plasticity and evenly distributed shear deformation developed at the whole steel web panel can be assumed.

3.4. Strength and stiffness degradations

It can be observed that the strength of the joint specimen may decrease at the same displacement level. The strength degradation coefficient λ, which is defined by dividing the ultimate load of the second cycle with the ultimate load of the first cycle at the same displacement amplitude [25], can be used to illustrate such degradation phenomena. The strength degradation coefficient λ versus normalized displacement $j = \Delta_j/\Delta_y$ curves of all the specimens are shown in Fig. 10a. For the specimens SRCTJ1, the strength

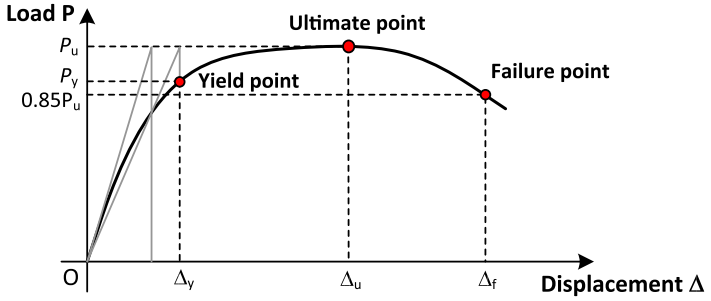

Fig. 8. Characteristic points on load–displacement curve.

Table 2
Summary of measured results.

Specimens	Loading direction	P_y (kN)	Δ_y (mm)	P_u (kN)	Δ_u (mm)	Δ_f (mm)	Ductility coefficient Δ_f/Δ_y
SRCTJ1-1	Positive	580.0	29.5	687.0	69.6	99.6	3.4
	Negative	620.0	24.5	693.2	46.4	91.3	3.7
SRCTJ1-2	Positive	575.0	27.0	672.2	52.3	83.4	3.1
	Negative	600.0	26.0	684.3	60.0	88.9	3.4
SRCTJ2-1	Positive	775.0	21.0	979.2	48.8	114.1	5.4
	Negative	750.0	17.5	1004.3	35.5	38.8	2.2[a]
SRCTJ2-2	Positive	770.0	21.0	974.5	50.5	115.6	5.5
	Negative	755.0	19.5	1000.8	46.3	47.0	2.4[a]

[a] *Note:* These values should be much lower than the actual values since the actual negative failure displacements are not achieved in the tests due to the limitation of the negative loading capacity of the actuator for the specimens SRCTJ2.

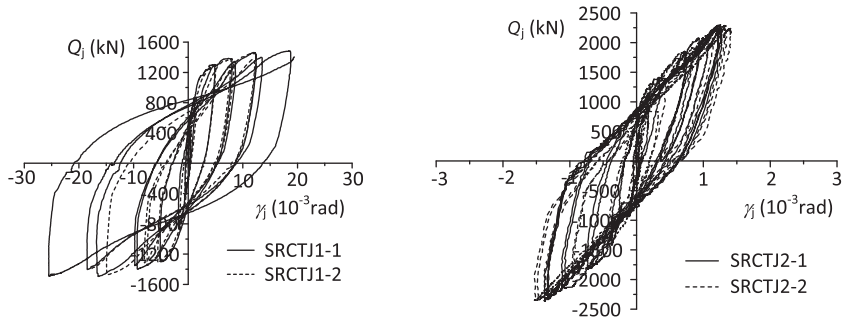

Fig. 9. Shear behavior of the joint core.

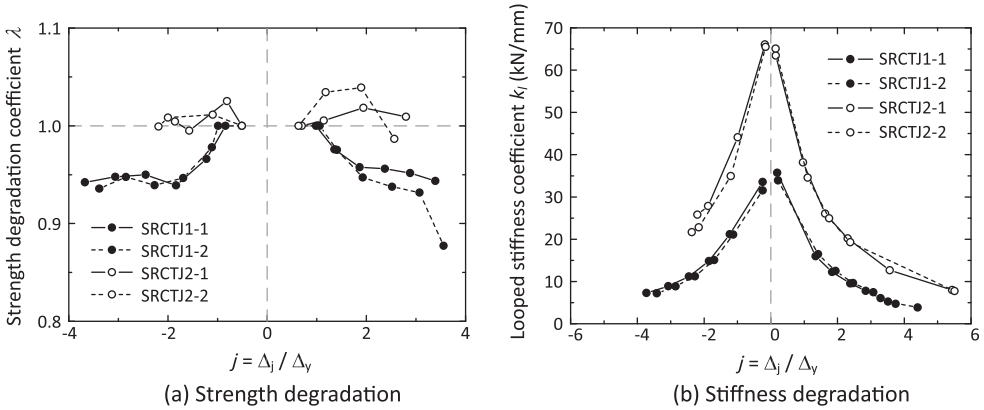

Fig. 10. Strength and stiffness degradations.

degradation can be evidently observed due to the concrete crushing of the joint core with the increasing of the displacement amplitude. On the contrary, a slight strength hardening phenomena can be observed for the specimens SRCTJ2 from the measured strength degradation coefficient λ exceeding 1.0 after the yielding of the specimens.

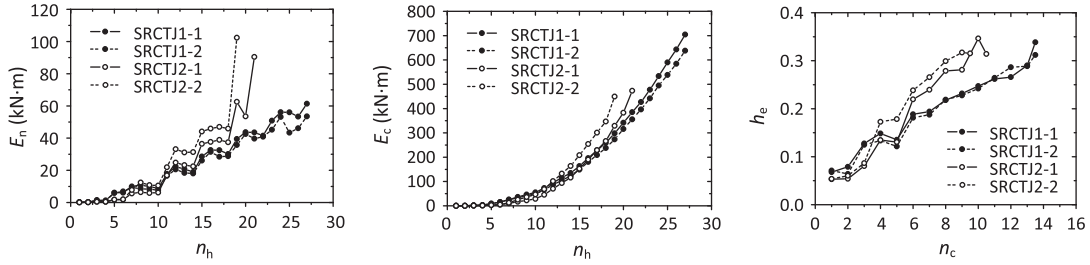

Fig. 11. Energy dissipation capacities of specimens.

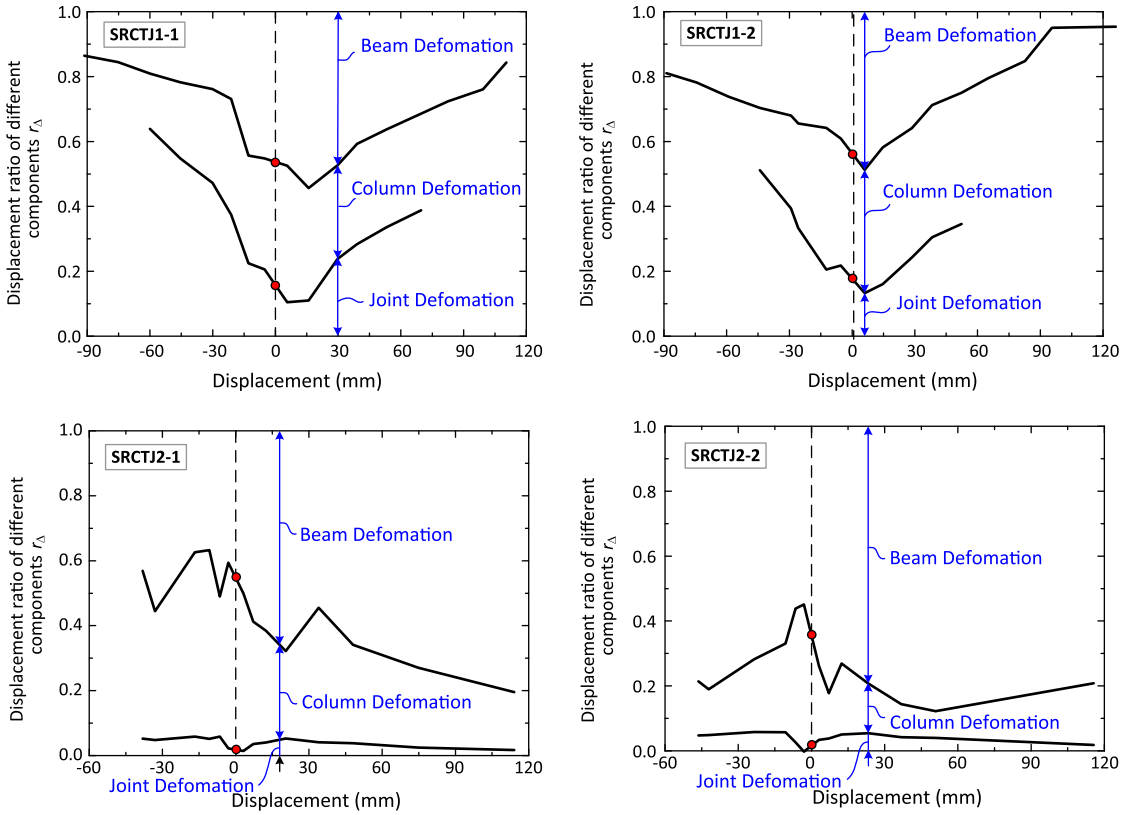

Fig. 12. Deformation analysis of specimens.

The looped cyclic stiffness k_l is used to describe the stiffness degradation of the specimens as shown in Fig. 10b, and the formula for calculating k_l can be found in Ref. [26] as

$$k_l = \sum_{i=1}^{n} P_j^i \Big/ \sum_{i=1}^{n} \Delta_j^i \tag{4}$$

where P_j^i and Δ_j^i are the maximum values of the load and the corresponding displacement under the ith cycle when the deformation is controlled as $\Delta_j = j \times \Delta_y$ and n is the number of cycles when the deformation is controlled as $\Delta_j = j \times \Delta_y$.

It can be clearly seen that the looped cyclic stiffness of all the specimens degrade evidently and stably during the entire loading process. The stiffness of the specimens SRCTJ2 with flexural failure at the beam end is much higher than that of the specimens SRCTJ1 with shear failure at the joint core. Therefore, rational control of the failure mode is one of the most effective ways to enhance the seismic behavior of the joint.

3.5. Ductility

Ductility is one of the most significant indexes to evaluate the seismic performance of a structure. The displacement ductility coefficient can be calculated as the ratio of failure displacement Δ_f to the yield displacement Δ_y. The displacement ductility coefficients of all the specimens listed in Table 2 indicate good ductility of all the specimens. It should be pointed out that due the limitation of the negative loading capacity of the actuator, the actual negative failure displacements of the specimens SRCTJ2 are not achieved in tests. Thus, the actual negative displacement ductility coefficients should be much larger than the experimental measurements for the specimens SRCTJ2, and the measured positive displacement ductility coefficients demonstrate that the ductility of the specimens SRCTJ2 is much better than that of the specimens SRCTJ1.

3.6. Energy dissipation capacity

Some critical indexes for evaluating the energy dissipation capacity are calculated from the load–displacement hysteretic

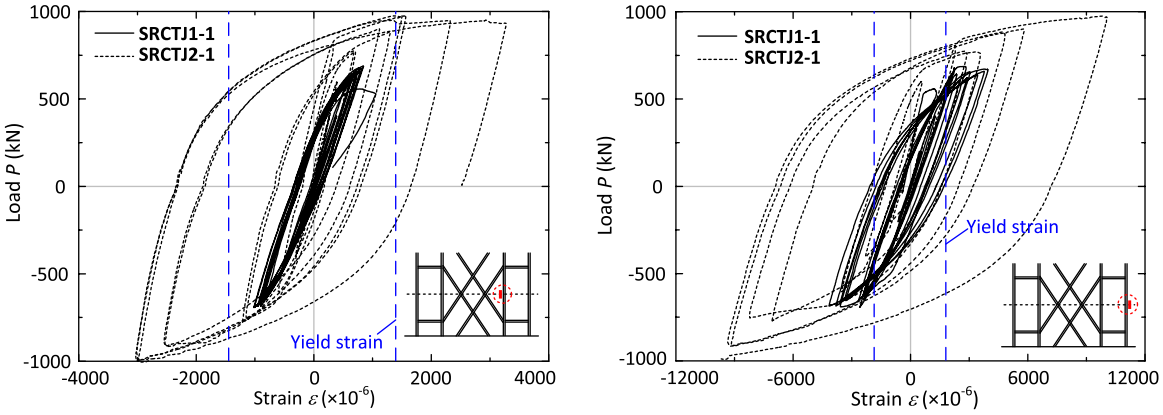

Fig. 13. Strain analysis at the critical beam-end section adjacent to the joint core.

loops and compared among all the specimens here. The E_n–n_h, E_c–n_h, and h_e–n_c curves are illustrated in Fig. 11, where E_n is the energy dissipated per hemicycles of the hysteretic loops, n_h is the number of hemicycles, E_c is the cumulative dissipated energy, h_e is the equivalent damping ratio [20], and n_c is the number of cycles. It can be seen that the energy dissipations are steadily and evidently enhanced with the increasing of cycle numbers after the specimens yield. Since the assessment of energy dissipation in SRCTJ2 is constrained by the limitation of the negative loading capacity of the actuator, the total number of cycles of SRCTJ2 is less than that of SRCTJ1 as shown in Fig. 11. However, it can still be observed from about the first 10 cycles (i.e., 20 hemicycles) that the specimens SRCTJ2 with flexural failure at the beam end illustrate better energy dissipation capacity than the specimens SRCTJ1 with shear failure at the joint core.

3.7. Deformation analysis

The ratios of the three deformation components including beam deformation, column deformation and joint deformation to the total deformation are calculated using Eqs. (1)–(3) in Section 2.4 and plotted in Fig. 12.

At the initial loading stage, the displacement ratio due to the joint deformation is the smallest for all the four specimens. For the specimens SRCTJ1, the displacement ratio due to the joint deformation increases most quickly in the loading process and reaches almost 60% at the end of the test, indicating the joint failure at the ultimate limit state. For the specimens SRCTJ2, the displacement ratio due to the beam deformation increases most quickly in the loading process and reaches almost 80% at the end of the test, indicating the beam-end failure at the ultimate limit state.

3.8. Flexural behavior at steel truss beam end

The strains of the two chords of the steel truss beam at a critical section adjacent to the joint core are monitored to investigate the beam-end flexural behavior, and some representative results are illustrated in Fig. 13. The inner flange of the chord at the beam-end section of the specimen SRCTJ1-1 is still in the elastic stage when the joint fails while that of the specimen SRCTJ2-1 yields with the maximum strain of about 3200 με as shown in Fig. 13a. Although the outer flange of the chord at the beam-end section of the both specimens SRCTJ1-1 and SRCTJ1-2 yields when the joint fails, evidently deeper plasticity of SRCTJ2-1 with the maximum strain of about 10,000 με is developed than that of SRCTJ1-1. As a result, at the ultimate limit state of the joint, partial plasticity is achieved at the beam end for the SRCTJ1 series, and a flexural plastic hinge in full plasticity is formed at the beam end for the SRCTJ2 series.

4. Shear strength of the joint core

The shear strength of the joint core can be evaluated using the strength superposition method. Namely, the shear strength contributed by the concrete and the steel are first calculated separately, and then the two strength components are superposed to obtain the joint shear strength. Although the shear model of the steel reinforced concrete column–steel truss beam joint core has been rarely investigated, the researches on the steel reinforced concrete column–steel solid web beam (SRC–S) joint core or some other similar types of hybrid joint core such as the reinforced concrete column–steel solid web beam (RC–S) joint core can be referred to in the present study.

Among the models available in the literature, the formulae for predicting the shear strength contributed by the steel are similar. However, different models for predicting the shear strength contributed by the concrete are provided by different researches and design codes. The compression field model and compression strut model are the two representative models reflecting two different shear mechanisms of the core concrete. The equations for the compression field model are similar to those used to calculate the shear strength in reinforced concrete beams so that the strength contribution of the stirrups in the joint core should be considered. While in the compression strut model, only the compressive strength of the core concrete dominates the shear strength and the strength contribution of the stirrups can be neglected. When the compression field model or the compression strut model is used separately to model the whole joint core [23,27], the complex mechanism of the composite effect between the steel and concrete for the hybrid joint core may be insufficiently reflected. As a result, some more complex models such as the inner compression strut-outer compression field model [9] and the inner compression strut-outer compression strut model [14] can be used to more reasonably model the shear behavior of the concrete at the hybrid joint core. Based on the experimental observations, the inner compression strut-outer compression strut model is selected here to predict the shear strength contributed by the core concrete for the steel reinforced concrete column–steel truss beam hybrid joint.

4.1. Equilibrium of ultimate external forces and internal shear strengths

The shear force at the joint core results from externally applied loads, and loads applied to the joint core are equivalent to the member forces adjacent to the joint. For design purposes, the shear strength of the joint core should be related to the ultimate member forces adjacent to the joint core based on the equilibrium conditions in consideration of the ultimate limit state. The forces on a typical subassembly are shown in Fig. 14a, and the relationship between the ultimate force at the beam inflection point and the shear strength at the joint core is derived here.

The equilibrium of the horizontal forces yields the following equilibrium equation:

$$\tau_{uj,i} h_{c,i} b_{e,i} = \frac{M_{bV,i}}{h_{b,i}} - V_{cV,i} \tag{5}$$

where $\tau_{uj,i}$ is the effective shear strength at the joint core for the ith strength component (i = 1 for the inner concrete compression strut; i = 2 for the outer concrete compression strut; and i = 3 for the steel web panel as shown in Fig. 14b); $h_{c,i}$, $h_{b,i}$ and $b_{e,i}$ are the width, depth, and thickness of the joint core region, respectively, for the ith strength component as shown in Fig. 14b; $V_{cV,i}$ is the ultimate shear force at the column inflection point corresponding to the shear failure at the joint core for the ith strength component; and $M_{bV,i}$ is the ultimate beam-end bending moment corresponding to the shear failure at the joint core for the ith strength component, calculated as:

$$M_{bV,i} = \frac{1}{2} V_{bV,i} (H_b - h_{c,i}) \tag{6}$$

where $V_{bV,i}$ is the ultimate shear force at the beam inflection point corresponding to the shear failure at the joint core for the ith strength component and H_b is the distance between the two adjacent beam inflection points.

The moment equilibrium around the central point O of the joint core region shown in Fig. 14a gives the following equation:

$$V_{cV,i} = \frac{H_b}{2H_c} V_{bV,i} \tag{7}$$

where H_c is the distance between the two adjacent column inflection points.

By introducing Eqs. (6) and (7) into Eq. (5), the expression of the ultimate shear force at the beam inflection point when the shear

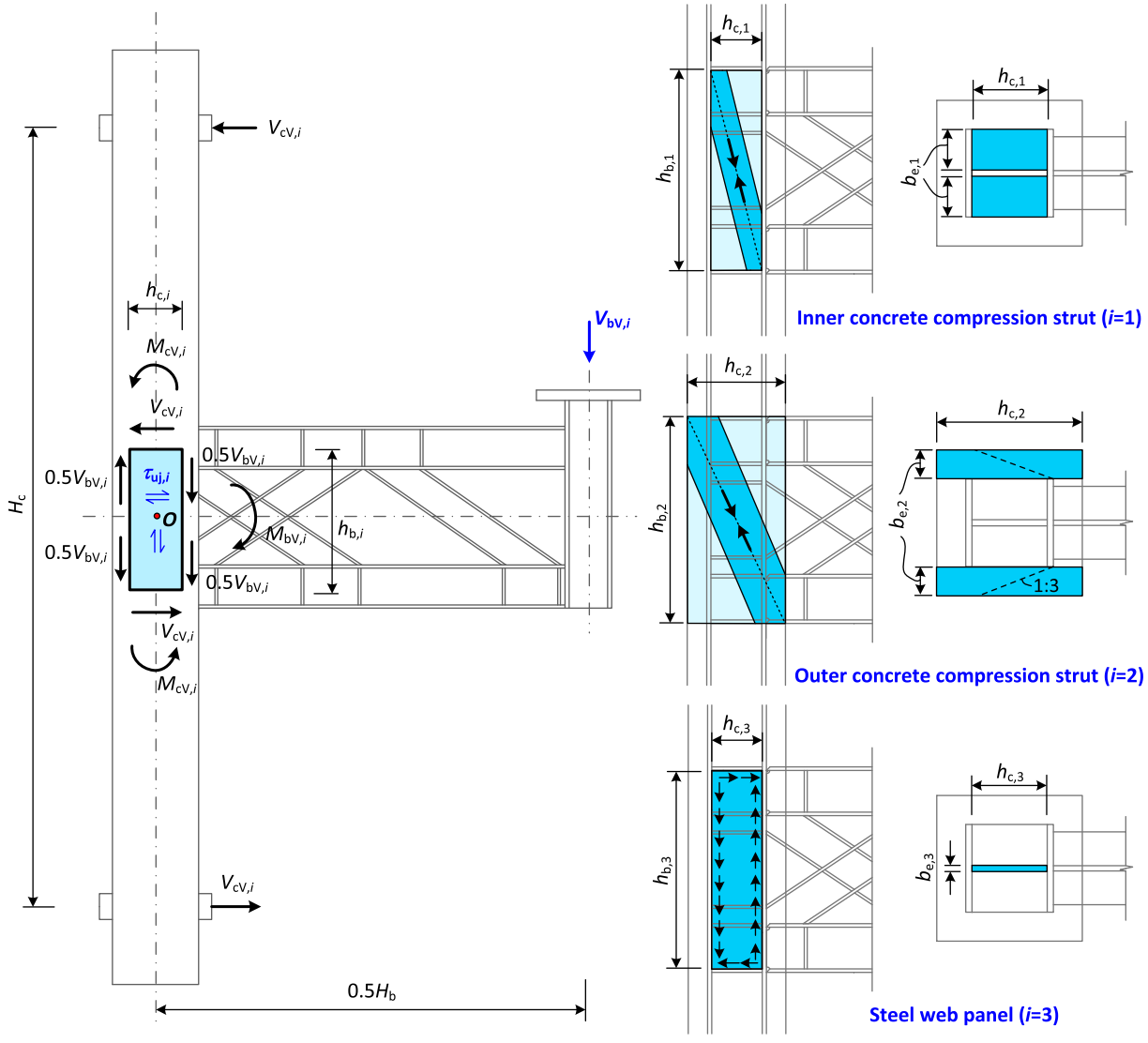

(a) Equilibrium of ultimate external forces and internal strengths

(b) Three components of shear strength

Fig. 14. Model for shear strength of the joint core.

strength of the joint core is achieved for the ith strength component $V_{bV,i}$ can be obtained as:

$$V_{bV,i} = \frac{2\tau_{uj,i}h_{c,i}h_{b,i}b_{e,i}H_c}{H_bH_c - H_ch_{c,i} - H_bh_{b,i}} \quad (8)$$

Through the superposition of the three strength components, the ultimate shear force at the beam inflection point due to the shear failure at the joint core V_{bV} can be finally calculated as:

$$V_{bV} = \sum_{i=1}^{3} V_{bV,i} \quad (9)$$

In addition to the equilibrium of the horizontal forces, the equilibrium of the vertical forces as Eq. (10) can also be used to derive the relationship between the ultimate shear force at the beam inflection point and the shear strength at the joint core.

$$\tau_{uj,i}h_{b,i}b_{e,i} = \frac{2M_{cV,i}}{h_{c,i}} - \frac{1}{2}V_{bV,i} \quad (10)$$

Introducing the following equation into Eq. (10) can give the same expression of $V_{bV,i}$ as Eq. (8). As a result, the two different derivation approaches finally achieve the same formula.

$$2M_{cV,i} = \frac{1}{2}V_{bV,i}H_b - V_{cV,i}h_{b,i} = \frac{1}{2}V_{bV,i}\left(H_b - \frac{H_b}{H_c}h_{b,i}\right) \quad (11)$$

4.2. Effective shear strengths for three mechanisms

As shown in Fig. 14b, three mechanisms are assumed to contribute to the shear strength of the joint core: (1) an inner concrete compression strut mechanism; (2) an outer concrete compression strut mechanism; and (3) a steel web panel shear mechanism. The determinations of the effective shear strengths corresponding to these three different mechanisms are discussed here.

4.2.1. Inner concrete compression strut

The inner concrete compression strut mechanism is activated by bearing of the column steel flanges and column web stiffeners. The inner compression strut is approximately assumed to have a depth equal to 30% of its length [14,28] so that the effective shear strength contributed by the inner concrete compression strut mechanism $\tau_{uj,1}$ can be calculated as

$$\tau_{uj,1} = 0.3f_c'k_{c1}\beta_1 \quad (12)$$

where f_c' is the cylinder compressive strength of the core concrete, determined as 0.8 of the cubic compressive strength f_{cu}; k_{c1} is factor for considering the effect of confinement on the inner strut strength selected as 2 proposed by Elnashai and Elghazouli [29] for steel-encased sections; and β_1 is the softening parameter for considering the effect of cracking on the inner strut strength calculated as Eq. (13) proposed by Vecchio and Collins [30].

$$\beta_1 = \frac{1}{0.85 + 0.27k_{tc1}} \quad (13)$$

where k_{tc1} is the ratio of principal tensile and compression strains, selected as 3 due to the significant cracking of the joint core at the ultimate limit state [14].

4.2.2. Outer concrete compression strut

The outer concrete compression strut mechanism is activated by transfer of forces from the upper and lower chords of the steel truss beam to the outer joint core regions through the steel column as a shear key. The depth of the outer compression strut is also assumed to be equal to 30% of its length, and the formula for effective shear strength contributed by the outer concrete compression strut mechanism $\tau_{uj,2}$ as Eq. (14) is similar to that contributed by the inner concrete compression strut mechanism.

$$\tau_{uj,2} = 0.3f_c'k_{c2}\beta_2 \quad (14)$$

where the factor k_{c2} is assumed to be 1 due to the slight confinement effect of the outer strut concrete; and the softening parameter for considering the effect of cracking on the outer strut strength β_2 is selected as the same value as β_1 for the inner concrete strut.

4.2.3. Steel web panel

Based on the previous researches on RC–S and SRC–S hybrid joints, the effective shear strength contributed by the steel web panel shear mechanism $\tau_{uj,3}$ can be calculated as

$$\tau_{uj,3} = 0.6k_wf_{ycw} \quad (15)$$

where f_{ycw} is the yield strength of the steel web panel; and the effective coefficient k_w can be selected as different values with different assumptions as summarized in Table 3. If the full plasticity is assumed, k_w can be selected as 1.0 as proposed by many researchers and design codes (e.g., Chen et al. [31]; Chen and Lin [27]; Cheng and Chen [15]; AISC [32]; ASCE Task Committee on Design Criteria for Composite Structures in Steel and Concrete [9]; and JCI [33]). In some researches, the partial plasticity model was proposed so that

Table 3
Values of the effective coefficient k_w in the literature.

Assumptions	References	Effective coefficient k_w
Full plasticity is developed at the web panel	Chen et al. [31]	1.0
	Chen and Lin [27]	1.0
	Cheng and Chen [15]	1.0
	AISC [32]	1.0
	ASCE Task Committee on Design Criteria for Composite Structures in Steel and Concrete [9]	1.0
	JCI [33]	1.0
Partial plasticity is developed at the web panel	Parra-Montesinos et al. [12]	0.9 (interior joint)
	Parra-Montesinos and Wight [14]	0.8 (exterior joint)
	Kim and Noguchi [34]	0.83
	Sakaguchi [35]	0.9
Contribution of the web strain hardening and the transverse flanges are considered	AISC [32]	$1 + (3 \times b_{cf} \times t_{cf}^2)/(h_b \times h_{cs} \times t_{cw})$[a] = 1.06(SRCTJ1) and 1.02(SRCTJ2)
	Chen and Lin [27]	
	Chou and Uang [20]	
	AIJ [23]	1.2

[a] *Note:* b_{cf} is the width of the column flange; t_{cf} the thickness of the column flange; h_b the depth of steel truss beam; h_{cs} the depth of column steel; and t_{cw} is the thickness of the steel web panel.

Table 4
Predictions of ultimate loading capacity and failure mode of the specimens.

Specimens	$V_{bV,1}$ (kN)	$V_{bV,2}$ (kN)	$V_{bV,3}$ (kN)	V_{bV}(kN)	V_{bM} (kN)	Failure mode	Failure mode[a]	V_b (kN)	V_b[a] (kN)		V_b/V_b[a]
SRCTJ1-1	222.2	170.8	282.6	675.7	819.2	SJ	SJ	675.7	(+)	687.0	0.983
									(−)	693.2	0.975
SRCTJ1-2	222.2	170.8	282.6	675.7	819.2	SJ	SJ	675.7	(+)	672.2	1.005
									(−)	684.3	0.987
SRCTJ2-1	695.2	365.9	858.3	1919.4	906.8	FB	FB	906.8	(+)	979.2	0.926
									(−)	1004.3	0.903
SRCTJ2-2	737.8	388.3	858.3	1984.4	906.8	FB	FB	906.8	(+)	974.5	0.931
									(−)	1000.8	0.906
Average											0.952
Standard deviator											0.037

[a] Represents the experimental results and no superscript represents the analytical predictions.

Table 5
Comparison of different formulas for predicting the shear strength of the joint core of SRCTJ1.

Reference	$\tau_{uj,1}$	$h_{c,1}$	$h_{b,1}$	$b_{e,1}$	$\tau_{uj,2}$	$h_{c,2}$	$h_{b,2}$	$b_{e,2}$	$\tau_{uj,3}$	$h_{c,3}$	$h_{b,3}$	$b_{e,3}$	V_{bV} (kN)	V^*_{bV} (kN)	V_b/V^*_b
JCI [33] ***Compression strut***	$1.07 \times 0.5 \times 0.3f'_c$	h_c	h_b	b_c	–	–	–	–	$0.6f_{ycw}$	h_{cw}	$h_b - 2t_{bf}$	t_{cw}	664.2	684.2	**0.971**
ASCE Task Committee on design criteria for composite structures in steel and concrete [9]: ***Inner compression strut-outer compression field***	$1.7\sqrt{f'_c} \leqslant 0.5f'_c \frac{h_{b,1}}{h_{c,1}}$	h_{cw}	$h_b - 2t_{bf}$	$b_{cf} - t_{cw}$	$0.4\sqrt{f_{c'}} + \frac{0.9A_{sh}f_{ys}}{b_{e,2}s_h} \leqslant 1.7\sqrt{f_{c'}}$	h_c	h_b	$b_c - b_{cf}$	$0.6f_{ycw}$	h_{cw}	$h_b - 2t_{bf}$	t_{cw}	627.7	684.2	**0.917**
Parra-Montesinos and Wight [14]: ***Inner compression strut-outer compression strut***	$0.3 \times 0.7f'_c \times(-0.0048f'_c + 1.13)$	h_{cw}	$h_b - 2t_{bf}$	$b_{cf} - t_{cw}$	$0.3 \times 0.34f'_c \times(-0.0048f'_c + 1.13) \times 1.1$	h_c	h_b	$b_c - b_{cf}$	$0.6 \times 0.8 \times f_{ycw}$	h_{cw}	$h_b - 2t_{bf}$	t_{cw}	453.2	684.2	**0.662**
Proposed: ***Inner compression strut-outer compression strut***	$0.3 \times 2 \times \beta_1 f'_c$	h_{cw}	$h_b - 2t_{bf}$	$b_{cf} - t_{cw}$	$0.3 \times \beta_2 f'_c$	h_c	h_b	$b_c - b_{cf}$	$0.6f_{ycw}$	h_{cw}	$h_b - 2t_{bf}$	t_{cw}	675.7	684.2	**0.988**

Note: h_c is the depth of column; h_b the depth of steel truss beam; h_{cw} the depth of column steel web; b_c the width of column; b_{cf} the width of column steel flange; t_{bf} the thickness of steel truss beam flange; t_{cw} the thickness of steel web panel; A_{sh} the area of joint stirrups parallel to the steel truss beam; f_{ys} the yield strength of the ties; s_h the vertical spacing between the horizontal stirrups; and $\beta_1 = \beta_2$ is the softening parameter for considering the effect of cracking calculated as Eq. (13).
V_{bV} is the analytical predictions of ultimate shear force at the beam inflection point of SRCTJ1 with shear failure at the joint core and V^*_{bV} is the average experimental result of ultimate shear force at the beam inflection point of SRCTJ1 with shear failure at the joint core.

the effective coefficient k_w was assumed smaller than 1.0 (e.g., Parra-Montesinos et al. [12,14] selected 0.9 for interior joints and 0.8 for exterior joints; Kim and Noguchi [34] selected 0.83; and Sakaguchi [35] selected 0.9). The value larger than 1.0 for k_w can also be found in the literature since the contribution of the web strain hardening and the transverse flanges are considered. AIJ [23] provided a constant value of 1.2, and AISC [32] proposed a more complex formula (Table 3), which yields 1.06 for SRCTJ1 and 1.02 for SRCTJ2.

Since the full plasticity has been observed at the steel web panel in the experiment program as discussed in Section 3.3, a constant and simple value of 1.0 is selected here for the effective coefficient k_w just like many other similar researches.

4.3. Verification and discussion

The ultimate shear forces of the specimens at the beam inflection point due to the shear failure at the joint core V_{bV} can be calculated using the proposed superposition method presented in the last section. The predictions of V_{bV} for all the four specimens are listed in Table 4. In addition to the shear failure at the joint core (represented as SJ in Table 4), the flexural failure at the truss beam end (represented as FB in Table 4) can also be observed in the tests. The ultimate shear force at the beam inflection point due to the flexural failure at the truss beam end V_{bM} can be obtained by assuming that the plasticity is fully developed at the critical section of the beam adjacent to the joint core. The actual ultimate shear force at the beam inflection point V_b can be determined as the minimum value of V_{bV} and V_{bM}, and the corresponding failure mode is the actual failure mode of the joint subjected to the earthquake action. This analytical procedure is applied to all the tested specimens as shown in Table 4. The predicted failure modes agree with the experimental results, and the ultimate loading capacity of the joint can be predicted with good accuracy. As a result, when the proposed analytical method is adopted, the failure mode of the joint can be effectively controlled to achieve the strong joint core/weak member design goal.

Several available formulas provided in the current design codes and the literature are compared with the proposed formula in this paper for predicting the ultimate shear force at the beam inflection point of SRCTJ1 as shown in Table 5. The proposed formula derived using the inner compression strut-outer compression strut model in this paper gives the most accurate result among all the four formulas, and the formula based on the compression strut model provided by JCI [33] also demonstrates good accuracy. However, the formula proposed by ASCE Task Committee on Design Criteria for Composite Structures in Steel and Concrete [9] using the inner compression strut-outer compression field model may underestimate the shear strength of the joint core. In addition, the design formulaproposed by Parra-Montesinos and Wight [14] for exterior standard RC–S hybrid joints with hoops without transverse beams also underestimates the shear strength of the investigated joint core in the present study although the similar inner compression strut-outer compression strut model was used in their study.

Furthermore, the contributions of three mechanisms to the shear strength of the joint core can also be quantitatively evaluated as shown in Fig. 15. It can be clearly seen that for the tested specimens in this paper, the concrete (including inner compression strut and outer compression strut) contributes to about 55–60%

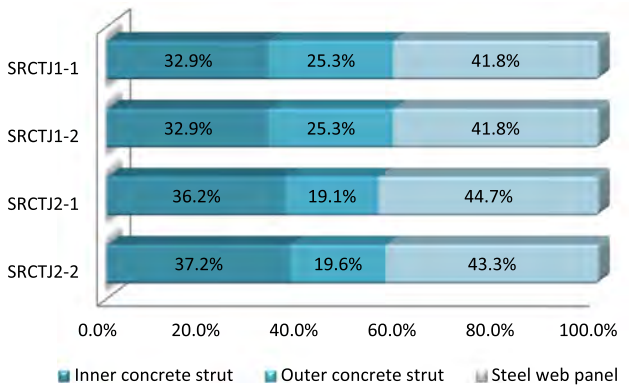

Fig. 15. Contributions of three mechanisms to the shear strength of the joint core.

of the total shear strength of the joint core while the steel web panel contributes to about 40–45%.

5. Conclusions

This paper presents an experimental and analytical research on the seismic behavior of the steel reinforced concrete column–steel truss beam hybrid joint.

In the experimental program, the structural mechanisms and failure modes of the joint are intensively investigated. The joints with flexural failure at the beam end illustrate higher stiffness and strength, better ductility and energy dissipation capacity than those with shear failure at the joint core. The composite action can be achieved through the natural cohesion between the steel and concrete for the steel reinforced concrete column in the hybrid subassembly no matter whether the shear studs are arranged or not.

In the analytical research, a design formula for shear strength of the joint core and an analytical method for controlling the failure mode of the joint are proposed using the shear model including inner concrete compression strut, outer concrete compression strut and steel web panel shear mechanisms. The proposed formula can more accurately predict the actual shear strength of the test joints compared with some other methods proposed in the literature and the current design codes, and the formula provided by JCI [28] also demonstrates good accuracy. The proposed design method in this paper can be used to quantitatively evaluate the contributions of different mechanisms to the shear strength of the joint core, and to effectively achieve the strong joint core/weak member design goal in the design practice.

Acknowledgments

The writers gratefully acknowledge the financial support provided by Key Project in the National Science & Technology Pillar Program during Twelfth Five-year Plan Period (Grant No. 2011BAJ09B01) and China Postdoctoral Science Foundation (Grant No. 2012M520287).

References

[1] Park HG, Hwang HJ, Lee CH, Park CH, Lee CN. Cyclic loading test for concrete-filled U-shaped steel beam–RC column connections. Eng Struct 2012;36:325–36.
[2] Parra-Montesinos GJ, Dasgupta P, Goel SC. Development of connections between hybrid steel truss–FRC beams and RC columns for precast earthquake-resistant framed construction. Eng Struct 2005;27(13):1931–41.
[3] Park WS, Yun HD. Bearing strength of steel coupling beam connections embedded reinforced concrete shear walls. Eng Struct 2006;28(9):1319–34.
[4] Henriques J, da Silva LS, Valente IB. Numerical modeling of composite beam to reinforced concrete wall joints Part I: calibration of joint components. Eng Struct 2013;52:747–61.
[5] Zhang YF, Zhao JH, Cai CS. Seismic behavior of ring beam joints between concrete-filled twin steel tubes columns and reinforced concrete beams. Eng Struct 2012;39:1–10.
[6] Sheikh TM, Deierlein GG, Yura JA, Jirsa JO. Beam–column moment connections for composite frames: Part 1. ASCE J Struct Eng 1989;115(11):2858–76.
[7] Deierlein GG, Sheikh TM, Yura JA, Jirsa JO. Beam–column moment connections for composite frames: Part 2. ASCE J Struct Eng 1989;115(11):2877–96.
[8] Kanno R, Deierlein GG. Strength, deformation, seismic resistance of joints between steel beams and reinforced concrete columns. Struct Eng Rep 1993:93–6. Cornell Univ, Ithaca, N.Y.
[9] ASCE Task Committee on Design Criteria for Composite Structures in Steel and Concrete. Guidelines for design of joints between steel beams and reinforced concrete columns. ASCE J Struct Eng 1994;120(8):2330–2357.
[10] Deierlein GG, Noguchi H. Overview of U.S.-Japan research on the seismic design of composite reinforced concrete and steel moment frame structures. ASCE J Struct Eng 2004;130(2):361–7.
[11] Parra-Montesinos G, Wight JK. Seismic response of exterior RC column-to-steel beam connections. ASCE J Struct Eng 2000;126(10):1113–21.
[12] Parra-Montesinos GJ, Liang X, Wight JK. Towards deformation-based capacity design of RCS beam–column connections. Eng Struct 2003;25(5):681–90.
[13] Fargier-Gabaldón LB, Parra-Montesinos JP. Behavior of reinforced concrete column–steel beam roof level T-connections under displacement reversals. ASCE J Struct Eng 2006;132(7):1041–51.
[14] Parra-Montesinos G, Wight JK. Modeling shear behavior of hybrid RCS beam–column connections. ASCE J Struct Eng 2001;127(1):3–11.
[15] Cheng CT, Chen CC. Seismic behavior of steel beam and reinforced concrete column connections. J Constr Steel Res 2005;61(5):587–606.
[16] Liang X, Parra-Montesinos GJ. Seismic behavior of reinforced concrete column–steel beam subassemblies and frame systems. ASCE J Struct Eng 2004;130(2):310–9.
[17] Nishiyama I, Kuramoto H, Noguchi H. Guidelines: seismic design of composite reinforced concrete and steel buildings. ASCE J Struct Eng 2004;130(2):336–42.
[18] Kuramoto H, Nishiyama I. Seismic performance and stress transferring mechanism of through-column-type joints for composite reinforced concrete and steel frames. ASCE J Struct Eng 2004;130(2):352–60.
[19] Noguchi H, Uchida K. Finite element method analysis of hybrid structural frames with reinforced concrete columns and steel beams. ASCE J Struct Eng 2004;130(2):328–35.
[20] Chou CC, Uang CM. Cyclic performance of a type of steel beam to steel-encased reinforced concrete column moment connection. J Constr Steel Res 2002;58(5–8):637–63.
[21] Weng CC, Yin YL, Wang HS, Yang CH. Experimental study on seismic performance of steel beam to SRC column connections. J Chin Inst Eng 2008;31(2):239–52.
[22] Seo SY, Yun HD, Kim SH. Structural resistance of SRC column–steel beam joint developed for innovative construction of buildings. J Iron Steel Res 2011;18(Suppl. 1–2):924–8.
[23] Architectural Institute of Japan (AIJ). AIJ standards for structural calculation of steel reinforced concrete structures and brief commentary, Tokyo, AIJ; 1991.
[24] Nie JG, Qin K, Cai CS. Seismic behavior of connections composed of CFSSTCs and steel–concrete composite beams: finite element analysis. J Constr Steel Res 2008;64(6):680–8.
[25] Han LH, Li W. Seismic performance of CFST column to steel beam joint with RC slab: experiments. J Constr Steel Res 2010;66(11):1374–86.
[26] Nie JG, Qin K, Cai CS. Seismic behavior of connections composed of CFSSTCs and steel–concrete composite beams: experimental study. J Constr Steel Res 2008;64(10):1178–91.
[27] Chen CC, Lin KT. Behavior and strength of steel reinforced concrete beam–column joints with two-side force inputs. J Constr Steel Res 2009;65(3):641–9.
[28] Tang JR, Chen XH. Behavior and calculation of shear capacity of steel reinforced concrete beam–column joint. J Build Struct 1990;11(4):28–36 [in Chinese].
[29] Elnashai AS, Elghazouli AY. Performance of composite steel/concrete members under earthquake loading. Part I: analytical model. Earthquake Eng Struct Dyn 1993;22(4):315–45.
[30] Vecchio FJ, Collins MP. Compression response of cracked reinforced concrete. ASCE J Struct Eng 1993;119(12):3590–610.
[31] Chen CC, Suswanto B, Lin YJ. Behavior and strength of steel reinforced concrete beam–column joints with single-side force inputs. J Constr Steel Res 2009;65(8–9):1569–81.
[32] American Institute of Steel Construction (AISC). Specification for structural steel buildings. Chicago (IL): AISC Inc.; 2005.
[33] Japan Concrete Institute (JCI). State of the art report of recent research and practice on composite and hybrid structures. Report of Research Committee on Composite and Hybrid Structures. Tokyo: Japan Concrete Institute; 1991.
[34] Kim K, Noguchi H. A study on the ultimate shear strength of connections with RC columns and steel beams. J Struct Constr Eng 1998;507:163–9. Architectural Institute of Japan (AIJ) [in Japanese].
[35] Sakaguchi N. Shear capacity of beam–column connection between steel beams and reinforced concrete columns. Trans AIJ 1991;428:69–77.